Cement & Concrete Composites 33 (2011) 12–18

Contents lists available at ScienceDirect

Cement & Concrete Composites

journal homepage: www.elsevier.com/locate/cemconcomp

Short-term creep of cement paste during nanoindentation

Christopher A. Jones, Zachary C. Grasley *

Zachry Department of Civil Engineering, Texas A&M University, College Station, TX 77845, United States

ARTICLE INFO

Article history:
Received 24 June 2010
Received in revised form 15 September 2010
Accepted 18 September 2010
Available online 24 September 2010

Keywords:
C–S–H
Creep
Viscoelastic
Nanoindentation

ABSTRACT

Current research interest in multi-scale modeling of cement paste requires accurate characterization of the time-dependent mechanical properties of the material, particularly the C–S–H phase. Nanoindentation is evaluated as a tool for measuring the short-term viscoelastic properties of cement paste. A time-dependent solution derived using the elastic–viscoelastic correspondence principle is used to characterize creep indentation tests performed on hardened cement paste and to extract the time-dependent properties. The effect of approximating C–S–H viscoelastic properties with a time-independent Poisson's ratio or time-independent bulk modulus is discussed, and arguments for utilizing a time-independent Poisson's ratio for short-term response are presented. The measured nanoindentation creep results indicate a trimodal trend both in the displacement versus time response of the test data and also in the extracted viscoelastic uniaxial compliance. Expressions for the mean short-term viscoelastic uniaxial compliance of C–S–H are given and a probability density function of the viscoelastic Young's modulus is plotted.

1. Introduction

In an effort to effectively model the multi-scale response of Portland cement concrete, experimental techniques are required that characterize the material on ever shorter length scales. In addition to providing intrinsic input properties for multi-scale models [1–5] for predicting the macroscale behavior of cement and concrete, measuring fundamental mechanical properties on the micro to nano scale enhances the understanding of concrete deformation mechanisms.

Nanoindentation involves the instrumented loading of a surface with a sharp probe while monitoring the applied force as a function of time, $P(t)$, and the displacement into the surface as a function of time, $h(t)$. While the nanoindentation technique has most often been used for determination of elastic properties, recently the technique has been applied to measure time-dependent mechanical properties as well.

Several studies have been conducted using the nanoindentation technique on cement and concrete to measure elastic properties. Velez et al. performed nanoindentation experiments on Portland cement clinker and measured properties for the main phases [6]. Multiple studies have investigated the elastic properties of hydrated Portland cement paste [7–13] in various experiments and calculations. Nanoindentation has also been used to measure elastic properties of phases in atypical cements and cement composites [14,15]. The existence of low density and high density C–S–H first proposed by Jennings and collaborators [16–18] was later utilized as an explanation for the bimodal distribution of elastic properties measured by Ulm and collaborators [19–21]. Trtik et al. [22] suggested that the presence of varying amounts of crystalline products (such as unhydrated cement or calcium hydroxide) within the nanoindentation interaction volume provide a more likely explanation for the measured bimodal distribution of elastic properties when ostensibly indenting C–S–H. Ulm et al. [23] suggested that large enough compositionally homogenous regions exist in hardened cement paste such that the nanoindentation interaction volume may often be a (compositionally) single phase so that the bimodal distribution of measured elastic properties in indentation of cement paste is explainable by two types of C–S–H. However, the exact microstructural phenomena dictating the multi-modal distribution of measured properties has not been definitively determined and is the subject of ongoing research.

While numerous studies have investigated the elastic properties of cement paste using nanoindentation, fewer studies have been conducted that investigate the nanoindentation technique as a tool for measuring viscoelastic properties of cementitious materials. Ulm and Vandamme provide solutions for the problem of time-dependent indentation and perform some experiments to validate the solutions [24,25]. Additionally, Vandamme and Ulm propose that the measured "creep modulus" indicates the presence of low density C–S–H, high density C–S–H, and an ultra-high density C–S–H [26]. Nemecek also considered nanoindentation creep as it affects the measured elastic properties of cement paste [27].

Some general solutions for time-dependent indentation also exist in the literature. Cheng et al. offers a viscoelastic solution for a

* Corresponding author. Tel.: +1 979 845 9961; fax: +1 979 458 0780.
E-mail addresses: C-Jones@ttimail.tamu.edu (C.A. Jones), zgrasley@civil.tamu.edu (Z.C. Grasley).

0958-9465/$ - see front matter © 2010 Elsevier Ltd. All rights reserved.
doi:10.1016/j.cemconcomp.2010.09.016

spherical indenter [28] and a flat punch indenter [29], neither of which extend well to more common conical indenters. Cheng and Cheng [30] also provide an excellent review of various phenomena present in indentation including indentation solutions for viscoelastic materials for constant displacement rate indentation tests. Other studies have been aimed at accounting for the viscoelastic dissipation that occurs when performing elastic indentations [27,31]. Fischer-Cripps [32] proposed a straightforward, phenomenological solution to characterize indentation creep, but the solution is empirical and thus not useful for understanding fundamental material behavior.

To date the application of time-dependent nanoindentation to cementitious materials has been limited. This study aims to characterize the short-term time-dependent viscoelastic Young's modulus of C–S–H using nanoindentation. Various assumptions made while formulating a time-dependent indentation solution will also be analyzed and a generalized solution for time-dependent indentation response of a viscoelastic material to a step loading will be presented.

2. Theory

A common method for deriving solutions to boundary value problems involving viscoelastic materials is the elastic–viscoelastic correspondence principle in which field variables and constitutive properties in an elastic solution are replaced by the corresponding Laplace (or Fourier) transformed viscoelastic analogs, solved in the transform domain, and then inverted back to the time domain. Unfortunately, the correspondence principle generally precludes problems that involve time-dependent transition from traction boundary conditions to displacement boundary conditions (or vice versa) on the boundary of the bodies involved. However, Lee and Radok [33,34] showed that transforms could be applied and accurate solutions obtained so long as the contact area between an indenter and the material being indented was monotonically increasing with time. In other words, for indenters of increasing cross-section with increasing contact depth, the correspondence principle could be used so long as the indenter probe was moving into the material, but not for the retraction. This method was used by Vandamme and Ulm [24] to create closed-form solutions for the indentation problem, which they applied to indentation tests of cement paste.

2.1. Background theory

The elastic solution for indentation of an isotropic solid considered in this analysis is the widely known Galin–Sneddon solution [35,36],

$$h^2(t) = \frac{\pi}{2\tan\theta}\frac{P(t)}{M}, \tag{1}$$

where $h(t)$ is the indentation depth as a function of time, θ is the half-angle of the conical indenter tip, $P(t)$ is the load as a function of time, and M is the indentation modulus defined as [37]

$$\frac{1}{M} = \frac{1-\nu^2_{material}}{E_{material}} + \frac{1-\nu^2_{indenter}}{E_{indenter}}, \tag{2}$$

where E is the elastic Young's modulus, ν is the Poisson's ratio, and the subscripts denote whether the property is of the indenter or of the material being indented. For diamond indenters ($E \sim 1$ TPa), the second term in (2) can be ignored such that

$$M \approx \frac{E_{material}}{1-\nu^2_{material}} = \frac{E}{1-\nu^2}. \tag{3}$$

Applying common intermoduli relations to (3) yields Eq. (10) of Ulm and Vandamme [24],

$$M = 4G\frac{3K+G}{3K+4G}, \tag{4}$$

where G is the shear modulus, and K is the bulk modulus of the body being indented.

2.2. Application of the correspondence principle

To apply (1) to the problem of creep indentation, all time-dependent parameters must be transformed to remove the time dependence. Once the relevant transformed parameters are obtained, the solution can be formed in the transform domain, and then this solution can be inverted back to the time domain. Substituting transformed parameters into (1) yields

$$\overline{h^2(s)} = \frac{\pi}{2\tan\theta}\frac{\overline{P(s)}}{s\overline{M(s)}}, \tag{5}$$

where the overbars denote the Laplace transformed quantity and s is the Laplace transform variable. Since an approximated step loading is applied in these experiments,

$$P(t) = P_{\max}H(t), \tag{6}$$

where $P_{\max}$ is the peak applied load and $H(t)$ is the Heaviside function. The Laplace transform of (6) is

$$\overline{P(s)} = \frac{P_{\max}}{s}, \tag{7}$$

and the Laplace transform of (3) is

$$s\overline{M(s)} = \frac{s\overline{E(s)}}{1-(s\overline{\nu(s)})^2}, \tag{8}$$

where the s-multiplication is necessary because of the differential operation in the constitutive equation of a linear viscoelastic material. The viscoelastic compliance $J(t)$ is related to the viscoelastic Young's modulus $E(t)$ in the transform domain as

$$\overline{E(s)} = \frac{1}{s^2\overline{J(s)}}. \tag{9}$$

Depending on the particular forms selected for $J(t)$ and $\nu(t)$ (or $K(t)$ and $G(t)$) the solution to the problem may not be analytically invertible into the time domain and a numerical inversion routine may be appropriate.

2.3. Approximating constant K or constant ν

The derivation presented in [24] holds K as constant (time-independent) and thereby assumes that the only time-dependent deformation is deviatoric. The indentation "creep modulus" reported in [26] is not utilized to determine traditional viscoelastic moduli, and thus the issue of approximating a constant K or ν is not broached. If $K(t)$ is approximated as constant, common intermoduli relations (applied in the transform domain) show that $\nu(t)$ must be an increasing function of time. The approximation of a constant value for $K(t)$ has precedent [38,39] since for most solid materials $G(t)$ relaxes faster than $K(t)$. For cementitious materials the literature seems to suggest that $\nu(t)$ may be approximated as a constant value [40–44] such that the relaxation rates for $K(t)$ and $G(t)$ are equal, although a study by Bernard et al. [45] indicates an increasing $\nu(t)$ (constant $K(t)$) after longer loading times. The question of constant ν seems to revolve around whether the material tested is behaving as a true isotropic solid or as a porous body [46]. No matter the externally applied traction on the boundary of a porous body, the internal state of stress in the solid phase is always mixed deviatoric and dilatational. Thus, we expect the relaxation rates of a highly porous body to be the same under applied hydrostatic or deviatoric stresses. With a nanoindenter, the

interaction volume of the cement paste tested is conservatively on the order of single digit cubic microns [8] and cement paste is known to contain substantial porosity in the nanometer range [17]. This nano-porosity contributes to a mixed stress state in the solid colloidal C–S–H particles, supporting the approximation of a constant $v(t)$, at least for short-term creep tests.

As will be shown in the results section, the average measured elastic Young's modulus in the indentation tests was $E = 21.6$ GPa. An assumed constant $v = 0.25$ combined with common intermoduli relations would suggest that $K = 7.57$ GPa. Based on [47,48], this calculated K agrees with that measured for the porous body of a typical hardened cement paste, not the bulk modulus of the solid phase (K_s), which is on the order of 45 GPa. The fact that the K calculated from the indentation experiments agrees with the value of K for a typical porous body of hardened cement paste suggests that the pore volume fraction in the indentation interaction volume is similar to the pore volume fraction in a bulk sample of hardened cement paste. Indeed, Vandamme and Ulm suggest C–S–H porosities ranging from 17% to 34%, depending on packing density of the particles [26]. Additional motivation for holding $v(t)$ constant is the insensitivity of the indentation modulus M to changes in v.

Vandamme and Ulm [26] suggest that the C–S–H creep mechanism is primarily nano-particle sliding. According to this proposed mechanism, an applied hydrostatic stress on a C–S–H colloidal mass results initially in a mixed dilatational and deviatoric stress state, but as deformation increases with time the packing density also increases. The result would be a gradual shift to purely dilatational stress state, and thus a purely dilatational response. As such, at later ages $v(t)$ will likely become an increasing function of time as the porosity of the material is reduced.

Because the durations of the creep tests performed in this research were short, in the analysis in this paper $v(t)$ will be held constant ($v = 0.25$) such that the Laplace transform of $v(t)$ is simply

$$\overline{v(s)} = \frac{0.25}{s}. \tag{10}$$

With the approximation that $v(t) = v(t = 0) = 0.25$, (5) can be fully defined in the transform domain and then inverted back to the time domain to give

$$h(t) = 1.21\sqrt{P_{\max}(J(t))\cot\theta}. \tag{11}$$

Eq. (11) will be used to fit the experimental data in subsequent sections.

3. Experimental

3.1. Materials and sample prep

The specimens used in this study were cast from a typical type I/II cement with a w/c of 0.4. The cement and water were mixed according to ASTM C305-99 and the resultant paste was then placed into acrylic tubes with a square cross-section and an inner dimension of 1 cm (0.394 in.). On one end, an acrylic plate was affixed with a two-part epoxy. The length of the tubes was approximately 10 cm (3.94 in.). The fresh paste filled molds were vibrated and vacuumed to remove any entrapped air. The specimens were then sealed and placed into a 98% relative humidity room at a temperature of 23 °C for 24 h. Once the initial curing had taken place, the specimens were carefully demolded and placed in lime water for approximately 90 days.

The cured "beams" were radially sliced across the long axis of the beam into 3 mm thick plates using an Isomet precision wet saw. The slices were allowed to dry in the laboratory environment and were then affixed with cyanoacrylate glue to circular steel discs measuring 15 mm (0.591 in.) in diameter. The exposed flat surface of the cement paste sample was polished using techniques similar to those presented in [49], with the addition of final polishing using diamond slurries in five steps with diamond particle sizes ranging from 6 μm to 0.25 μm. In these final steps the diamond slurry was placed on a glass plate and the specimen was manually oscillated against the glass. After each polishing step the specimen was wiped dry with denatured alcohol to remove any residue from the slurry.

3.2. Nanoindenter

In this study, a Hysitron Triboindenter model TI-900 was used for the creep indentation tests, which were conducted at room temperature (≈23 °C) and relative humidity (≈50% RH). The indenter was fitted with a typical diamond Berkovich indenter tip. For the creep loading, a trapezoidal shape load history was used in all cases which included a rapid load application phase with elapsed time t_l where the load was increased from $P = 0$ to $P = P_{\max}$, a load holding phase whose time was t_h, and an unloading phase whose time was t_u, where the load was reduced from $P = P_{\max}$ to $P = 0$. Since $t_h \gg t_l$, step loading was used as an approximation to simplify the analysis. Upon unloading, the penetration depth versus load was also monitored to determine the elastic properties for each test. The slope of the unloading curve was used in the Oliver and Pharr method [50] to determine the elastic indentation modulus.

3.3. Experimental design

The creep indentation tests performed in this study were all conducted at a single $P_{\max} = 1500$ μN to minimize any variability arising from the testing procedure. Two different holding times were used to assess the response of the material over different time scales. A total of 48 tests were conducted for the 30 s holding time and eight tests were conducted for the 1 h holding time. The results from four tests (of the forty-eight 30 s tests) were discarded; two tests lacked any time-dependent response (no creep) suggesting that the indentation occurred solely within a crystalline phase, and two tests were discarded due to erratic jumps in the displacement indicating crushing, fracture, or slipping. The fact that 52 of 56 total tests displayed some time-dependency in the measured response indicates that nearly all the indentation tests included some effect of C–S–H in the interaction volume. Test durations longer than 1 h were attempted, but the long-term thermal drift present in the nanoindentation measurement limited the value of the results.

To quantify the inherent drift present in the indenter in the 30 s and 1 h tests, a sample of polished sapphire was indented with identical load levels and holding times. In each batch of tests, an identical number of creep indentations were performed on the sapphire and on the cement. Since there is no reason to expect creep in the sapphire, any change in recorded indentation depth once the load reached its maximum level was attributed to drift. The average drift rate of the displacement for the 30 s creep tests was −0.0536 nm/s with a standard deviation of 0.00964 nm/s or a coefficient of variation of 18%. The total drift over a 30 s period was less than 3 nm. For the 1 h tests the displacement drift rate was −0.4316 nm/s with a standard deviation of 0.0286 nm/s and a coefficient of variation of 2%. For both the 30 s and 1 h creep tests of cement paste, the displacement response was adjusted to account for the drift rate.

4. Results

Once the corrected creep curves were obtained for the cement paste, the indentation depth with respect to time, $h(t)$, was plotted

and fitted with (11). The creep compliance function is assumed to be of the form of a stretched exponential [51], which has been used previously to fit short-term creep of cement paste [52]. A modified form of the stretched exponential function is

$$J(t) = \frac{1}{E_0} + \frac{1}{E_1(1-e^{-1})}\left(1 - e^{-(t/t_h)^{\beta}}\right), \tag{12}$$

where E_0, E_1, and β are fitting parameters. In the second term of (12), the presence of $(1 - e^{-1})$ in the denominator serves to normalize the entire term from 0 at $t = 0$ to $1/E_1$ at $t = t_h$. The form of creep compliance expressed in (12) was chosen because it fits data well with only a few fit parameters and the fit parameters possess physical meaning. When t_h is chosen to match the length of the load hold period of the test in question, the constitutive parameter E_0 controls the initial (instantaneous) elasto-plastic penetration into the material, E_1 controls the magnitude of the time-dependent penetration into the material over time t_h, and β controls the shape of the relaxation/retardation function. The parameter E_0 was determined using (1) and (3) with the initial measured loading depth at $t = t_i$. It is critical to note that this parameter is not equivalent to the elastic Young's modulus since the initial penetration almost certainly includes plastic deformation in addition to elastic deformation. The parameters E_1 and β were determined by fitting (11) with $J(t)$ expressed in (12) to the measured $h(t)$ using nonlinear regression. Fig. 1 shows a typical 30 s creep curve fitted with (11).

Table 1 shows a summary of the average fitted parameters for the 30 s load holding data and for the 1 h load holding data as well as the averages, standard deviations, coefficients of variation, and average r-squared value. By comparing the fit functions (11) evaluated at the mean values for E_0, E_1, and β for both the 30 s creep tests and the 1 h creep tests, the similarity between the functions can be shown. Fig. 2 shows (11) plotted with the mean values of E_0, E_1, and β obtained from both the 30 s and 1 h tests.

Fig. 2 shows that the increase in displacement plateaus after roughly 30–40 s for 1 h load holding time tests. This plateau in displacement seems to imply that the reduction in material stiffness also plateaus over this time frame, but this is not necessarily the case. For an indenter of increasing cross-sectional area with depth of penetration, the applied stress decreases with increasing penetration depth. Similar to the size effect discussed by Nemecek et al. [53], as the indenter creeps into the material the applied stress (under constant load) is reduced since the contact area increases with time. Various functions have been developed to characterize the contact area to penetration depth relationships for indenter tips. The contact area versus depth relationship generally obeys a parabolic relationship of the form

$$A(h) = C_0h^2 + C_1h^1 + C_2h^{1/2} + \ldots + C_nh^{1/(2^{n-1})}, \tag{13}$$

where $C_0 - C_n$ are tip specific parameters and h is the indentation depth. For a Berkovich indenter, $C_0 = 24.5$. If only the first term is considered and the average stress is assumed to be 1500 μN/A(h), then Fig. 3 shows the inverse relationship between average contact stress and contact area as a function of penetration depth over the realistic range of indentation depths encountered in these experiments.

Based on the results shown in Fig. 3, it is possible that the dissipation of the displacement rate shown in Fig. 2 is not due solely to a reduction in the creep rate, but rather a time-dependent reduction in applied stress. For a Berkovich tip with a half-angle of 70.32°, the reduction in stress occurs at a greater rate than for a sharper indenter tip (i.e. cube corner, cono-spherical, etc.). Though longer term creep data was obtained in this study with a Berkovich indenter and successfully fitted, performing long term

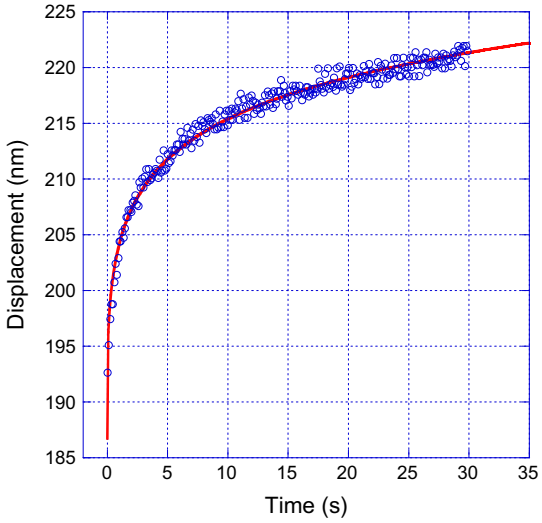

Fig. 1. Typical 30 s nanoindentation displacement versus time plot including the fit function. The data has been time shifted so that $t = t - t_i$.

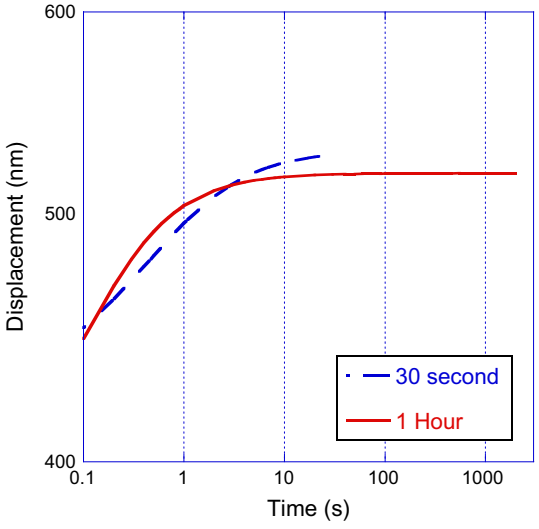

Fig. 2. The fit function $h(t)$ plotted using the mean values of E_0, E_1, and β calculated from the 30 s tests and from the 1 h tests.

Table 1
Fit parameters for the 30 s load holding data and for the 1 h load holding data.

	t_h = 30 s				t_h = 1 h			
	E_0	E_1	β	r^2	E_0	E_1	β	r^2
Average	10.772	27.311	0.280	0.987	10.342	2.038	0.755	0.898
Stand. dev.	5.202	14.261	0.026		1.536	2.851	0.242	
Coeff. of var. (*COV*)	0.483	0.522	0.092		1.115	1.399	0.321	

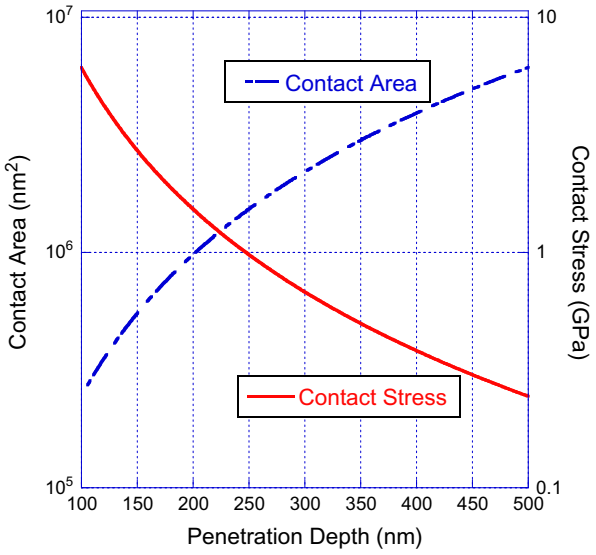

Fig. 3. For conical indenters, as the penetration depth (displacement) increases the contact area must increase, thus reducing the applied stress for a constant load. These curves assume a constant load of 1500 μN and a typical Berkovich indenter.

indentation creep tests with a sharper indenter may more accurately characterize the long term micro to nano scale creep response of the material and enable even longer term tests to be performed. Additionally, a quasi-static ramp load function instead of a step load function may also improve the viscoelastic characterization of cementitious materials for longer time periods since the reduction in stress would be partially offset by the increasing load.

In agreement with the trimodal distribution of measured elastic and viscoelastic responses recently reported by Vandamme and Ulm [26], many of the model fitting parameters obtained from fitting the measured indentation creep data with (11) also showed a trimodal trend. Fig. 4 shows the histograms for the fit parameters that indicate a trimodal response. A histogram of E, the elastic Young's modulus (calculated from the unloading slope) is also included in Fig. 4, and agrees well with data shown in [19]. The parameters E_0 and E_1 in particular demonstrate trimodal distributions. The trimodal response noted in this study could be attributed to varying quantities of low density (outer product) C–S–H, high density (inner product) C–S–H, and ultra-high density C–S–H within the indentation interaction volume, or it could be related to varying amounts of crystalline phases present in the interaction volume as shown in [8] and suggested by Trtik et al. [22]. Of particular interest is the trimodality of the parameter E_1, which suggests that there may be three distinct mechanisms facilitating the time-dependent response, that the three types of C–S–H proposed for the elastic case may have unique time-dependent responses, or that varying fractions of crystalline products in the interaction volume results in the trimodal viscoelastic response.

In addition to the trimodal trend noted in the individual fit parameters, a trimodal trend was also noted in the overall measured displacement response in the creep tests. As a way of analyzing this trend, the probability of measured indentation depth was analyzed. The probability of the response function (11) was decomposed as the sum of three overlaid Gaussian distributions as

$$P(h(t)) = aP(h(t)_{low}) + bP(h(t)_{medium}) + cP(h(t)_{high}), \tag{14}$$

where P is the probability and a, b, and c are linear multipliers that represent the fraction of each type of response (low, medium, or high deformation, respectively) such that $a + b + c = 1$. The variability of a function can be approximated using the delta method [54], where the function is approximated by a first order Taylor's series. The variance of the total function can be approximated as

$$Var(h_j(t,x_i)) = \sum_i \left(\frac{\partial h_j(t,\overline{x_i})}{\partial x_i}\right)^2 Var(x_i) + \frac{\partial^2 h_j(t,\overline{x_i})}{\partial x_i \partial x_k} Cov(x_i x_k), \quad i \neq k, \tag{15}$$

where $h_j(t, x_i)$ is the set of displacement functions for low, medium, or high deformation material, x_i is the set of fit parameters present in the function h_j (i.e. E_0, E_1, or β), $\overline{x_i}$ is the set of mean values computed for the fit parameters E_0, E_1, or β, and $Cov(x_i x_k)$ is the covariance between variables x_i and x_k. A significant covariance was found between E_0 and E_1, indicating that mechanisms or material structure that dictate the magnitude of E_0 likewise dictate the magnitude of E_1. With the variance for each function, and assuming a Gaussian probability distribution for each $h_j(t)$, the total probability density function (PDF) for the measured $h(t)$ can be formulated as

$$P(h(t)) = a\frac{1}{\sqrt{2\pi Var(h_{low}(t,\overline{x_i}))}} \exp\left[-\left(\frac{(h(t)-h_{low}(t,\overline{x_i}))^2}{2Var(h_{low}(t,\overline{x_i}))}\right)\right] + b\frac{1}{\sqrt{2\pi Var(h_{medium}(t,\overline{x_i}))}} \exp\left[-\left(\frac{(h(t)-h_{medium}(t,\overline{x_i}))^2}{2Var(h_{medium}(t,\overline{x_i}))}\right)\right] + c\frac{1}{\sqrt{2\pi Var(h_{high}(t,\overline{x_i}))}} \exp\left[-\left(\frac{(h(t)-h_{high}(t,\overline{x_i}))^2}{2Var(h_{high}(t,\overline{x_i}))}\right)\right], \tag{16}$$

where $a = 0.1219$, $b = 0.1953$, and $c = 0.6829$. The relative weighting of a, b, and c indicates that the high deformation response is most likely to be measured when indenting the material considered in this set of experiments. In contrast, Vandamme and Ulm [26] found that the medium deformation response was most probable for a material with a w/c of 0.3 and 25% calcareous filler. Based on the difference in the materials tested in this study and in [26], it is likely that the specimens tested in this study (w/c of 0.4) include a greater fraction of low density C–S–H (or less nanocrystalline inclusions in the C–S–H) in comparison to those tested by Vandamme and Ulm. This finding indicates that the viscoelastic response of C–S–H is controllable through material design at the nanoscale. A plot of (16) for the 30 s fit data, with the variance of the $h(t)$ functions approximated using (15), can be seen in Fig. 5a, which clearly shows a demarcation between high deformation (upper curve), medium deformation (middle curve), and low deformation (lower curve) responses, with the high deformation most probable. The probability of the viscoelastic Young's modulus, $E(t)$, was also calculated using the same procedure as for the displacement, with a plot of these results shown in Fig. 5b. The Gaussian PDF that yields the stiffest $E(t)$ (upper curve in Fig. 5b) influences the lowest deformation indentation response $h_{low}(t)$, the Gaussian probability PDF that yields the median $E(t)$ (middle curve in Fig. 5b) influences the median deformation indentation response $h_{medium}(t)$, and the Gaussian PDF that yields the most compliant $E(t)$ (lower curve in Fig. 5b) influences the high deformation indentation response $h_{high}(t)$. The lower coefficient of variation of $E(t)$ in the high stiffness regime causes $COV(h_{low}(t)) \ll COV(h_{high}(t))$, which tends to sharpen the Gaussian PDF of $h_{low}(t)$ in comparison to the Gaussian PDF of the upper curve of $E(t)$. Likewise, the Gaussian PDF of $h_{high}(t)$ is flattened versus the lower curve of $E(t)$.

5. Conclusions

Creep indentation tests have been performed on cement paste for two different durations. Following the solution of Ulm and

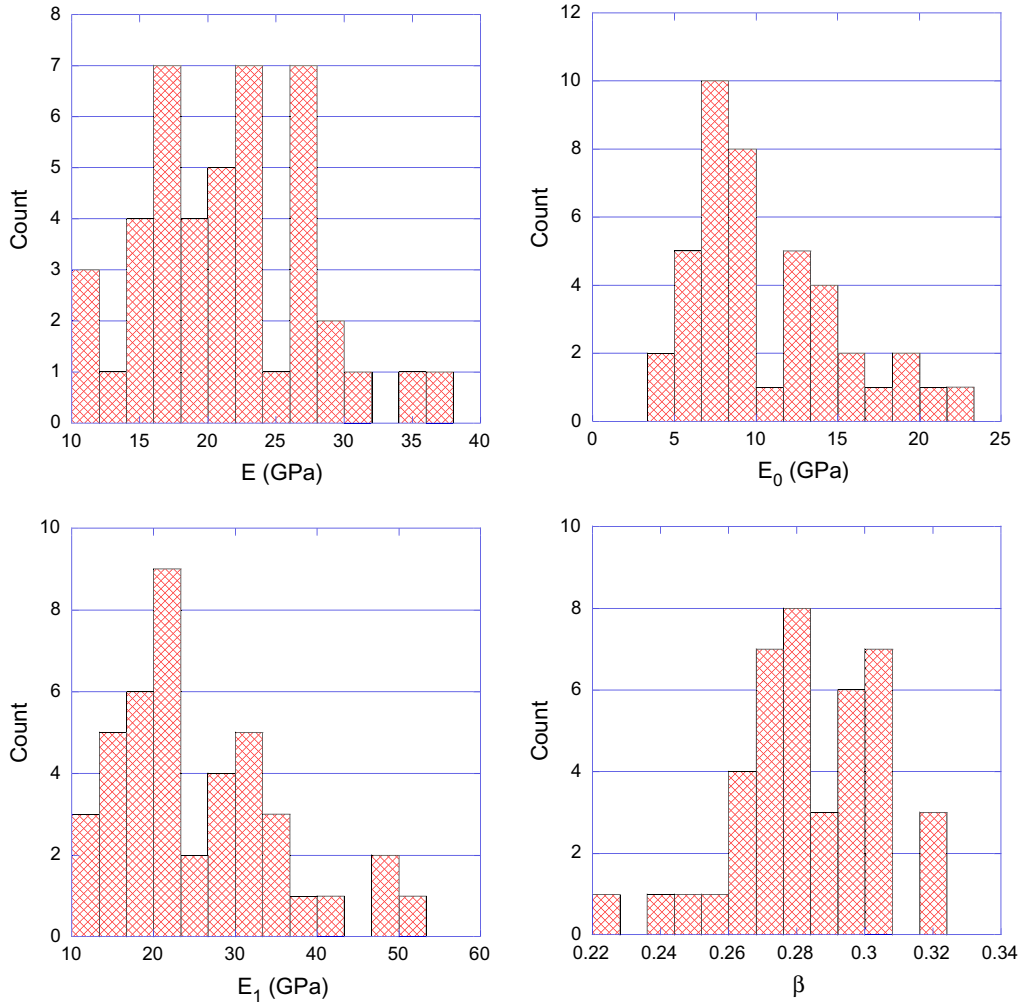

Fig. 4. Histograms for the fit parameters obtained from the 30 s creep indentation tests indicate a trimodal trend.

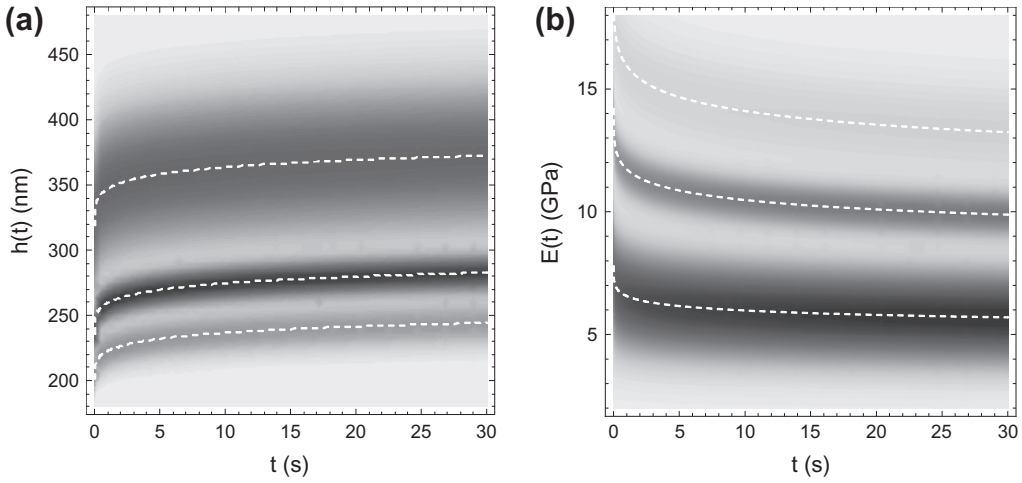

Fig. 5. The probability density plots of (a) $h(t)$ and (b) $E(t)$ showing the trimodal trend of measured displacements and viscoelastic properties extracted from the nanoindentation tests. Darker areas indicate higher probability, while dashed lines indicate mean values for each Gaussian probability density function.

Vandamme [24], but with the approximation of a constant value for viscoelastic Poisson's ratio, the displacement versus time data was fitted. The measured displacement data and fitted viscoelastic constitutive functions indicate that there is a trimodal trend present in the measured creep indentation results, although more testing may be necessary to fully confirm this observation. For the first time, expressions for the viscoelastic uniaxial compliance of C–S–H based on nanoindentation creep tests are reported; these expressions could be used in multi-scale models to predict short-term viscoelastic behavior of bulk cement paste.

Though creep relaxation appears to subside after a few tens of seconds in the 1 h tests, it is likely due in part to the decrease in applied stress as penetration depth increases. Unfortunately, this phenomenon may limit the applicability of the nanoindentation technique (with a Berkovich indenter) for long loading times and deep indentation depths. Despite this deficiency, the creep nanoindentation technique appears to be a viable experiment for characterizing the viscoelastic response of cementitious materials on a relatively short length scale.

Acknowledgements

This research was supported by the National Science Foundation Career Award Program under Grant Number CMMI-0843979. Any opinions, findings, and conclusions or recommendations expressed in this material are those of the author(s) and do not necessarily reflect the views of the National Science Foundation.

References

[1] Bullard JW, Garboczi EJ. A model investigation of the influence of particle shape on Portland cement hydration. Cem Concr Res 2006;36(6):1007–15.
[2] Ganneau FP, Ulm FJ, Gondzio J, Garboczi EJ. An algorithm for computing the compressive strength of heterogeneous cohesive-frictional materials – application to cement paste. Comput Geotech 2007;34(4):254–66.
[3] Garboczi EJ, Douglas JF, Bohn RB. A hybrid finite element-analytical method for determining the intrinsic elastic moduli of particles having moderately extended shapes and a wide range of elastic properties. Mech Mater 2006;38(8–10):786–800.
[4] Garboczi EJ, Haecker CJ, Bullard JW, Bohn RB, Sun Z, Shah SP, et al. Modeling the linear elastic properties of Portland cement paste. Cem Concr Res 2005;35(10):1948–60.
[5] Zhihui S, Garboczi EJ, Shah SP. Modeling the elastic properties of concrete composites: experiment, differential effective medium theory, and numerical simulation. Cem Concr Compos 2007;29(1):22–38.
[6] Velez K, Maximilien S, Damidot D, Fantozzi G, Sorrentino F. Determination by nanoindentation of elastic modulus and hardness of pure constituents of Portland cement clinker. Cem Concr Res 2001;31(4):555–61.
[7] Chandler MQ, Peters JF, Pelessone D. Modeling nanoindentation of calcium silicate hydrate. Transport Res Rec 2010;2(2142):67–74.
[8] Chen JJ, Sorelli L, Vandamme M, Ulm F-J, Chanvillard G. A coupled nanoindentation/SEM–EDS study on low water/cement ratio Portland cement paste: evidence for C–S–H/$Ca(OH)_2$ nanocomposites. J Am Ceram Soc 2010;93(5):1484–93.
[9] Hughes JJ. Micro-mechanical properties of cement paste measured by depth-sensing nanoindentation: a preliminary correlation of physical properties with phase type. 2–4th ed. USA: Elsevier; 2004. p. 223–31.
[10] Mondal P, Shah SP, Marks LD. Use of atomic force microscopy and nanoindentation for characterization of cementitious materials at the nanoscale. ACI SP 2008;254:41–56.
[11] Nemecek J, Kopecky L, Bittnar Z. Size effect in nanoindentation of cement paste. In: International conference on applications of nanotechnology in concrete design. Dundee (Scotland, United Kingdom): Thomas Telford Services Ltd.; 2005. p. 47–53.
[12] Sorelli L, Constantinides G, Ulm F-J, Toutlemonde F. The nano-mechanical signature of ultra high performance concrete by statistical nanoindentation techniques. Cem Concr Res 2008;38(12):1447–56.
[13] Zhu W, Hughes JJ, Bicanic N, Pearce CJ. Nanoindentation mapping of mechanical properties of cement paste and natural rocks. Mater Charact 2007;58(11–12):1189–98.
[14] Nemecek J, Smilauer V, Kopecky L, Nemeckova J. Nanoindentation of alkali activated fly ash. Transport Res Rec 2010;1(2141):36–40.
[15] Saez De Ibarra Y, Gaitero JJ, Erkizia E, Campillo I. Atomic force microscopy and nanoindentation of cement pastes with nanotube dispersions. Phys Status Solidi (A) Appl Mater 2006;203(6):1076–81.
[16] Jennings H. A model for the microstructure of calcium silicate hydrate in cement paste. Cem Concr Res 2000;30(1):101–16.
[17] Jennings H. Colloid model of C–S–H and implications to the problem of creep and shrinkage. Mater Struct 2004;37(1):59–70.
[18] Tennis PD, Jennings HM. Model for two types of calcium silicate hydrate in the microstructure of Portland cement pastes. Cem Concr Res 2000;30(6):855–63.
[19] Constantinides G, Ulm F-J. The effect of two types of C–S–H on the elasticity of cement-based materials: results from nanoindentation and micromechanical modeling. Cem Concr Res 2004;34(1):67–80.
[20] Jennings HM, Thomas JJ, Gevrenov JS, Constantinides G, Ulm F-J. A multi-technique investigation of the nanoporosity of cement paste. Cem Concr Res 2007;37(3):329–36.
[21] Ulm FJ, Constantinides G. The nanogranular nature of C–S–H. J Mech Phys Solids 2007;55(1):64–90.
[22] Trtik P, Munch B, Lura P. A critical examination of statistical nanoindentation on model materials and hardened cement pastes based on virtual experiments. Cem Concr Compos 2009;31(10):705–14.
[23] Ulm F-J, Vandamme M, Jennings HM, Vanzo J, Bentivegna M, Krakowiak KJ, et al. Does microstructure matter for statistical nanoindentation techniques? Cem Concr Compos 2010;32(1):92–9.
[24] Ulm FJ, Vandamme M. Viscoelastic solutions for conical indentation. Int J Solids Struct 2006;43(10):3142–65.
[25] Vandamme M. The nanogranular origin of concrete creep: a nanoindentation investigation of microstructure and fundamental properties of calcium–silicate–hydrates. Massachusetts Institute of Technology; 2008.
[26] Vandamme M, Ulm F-J. Nanogranular origin of concrete creep. Proc Natl Acad Sci 2009;106(26):10552–7.
[27] Nemecek J. Creep effects in nanoindentation of hydrated phases of cement pastes. Mater Charact 2009;60(9):1028–34.
[28] Cheng L, Xia X, Scriven L, Gerberich W. Spherical-tip indentation of viscoelastic material. Mech Mater 2005;37(1):213–26.
[29] Cheng L, Xia X, Yu W, Scriven L, Gerberich W. Flat-punch indentation of viscoelastic material. J Polym Sci, Part B: Polym Phys 2000;38(1):10–22.
[30] Cheng Y, Cheng C. Relationships between initial unloading slope, contact depth, and mechanical properties for conical indentation in linear viscoelastic solids. J Mater Res 2005;20(4):1046–53.
[31] Seltzer R, Mai Y. Depth sensing indentation of linear viscoelastic–plastic solids: a simple method to determine creep compliance. Eng Fract Mech 2008;75(17):4852–62.
[32] Fischer-Cripps AC. A simple phenomenological approach to nanoindentation creep. Mater Sci Eng, A 2004;385(1–2):74–82.
[33] Lee EH, Radok JRM. Contact problem for viscoelastic bodies. J Appl Mech Ser E 1960;27(3):438–44.
[34] Radok J. Visco-elastic stress analysis. Quart Appl Math 1957;15:198–202.
[35] Galin L, Sneddon I, Moss H. Contact problems in the theory of elasticity. Raleigh (NC): Dept. of Mathematics, School of Physical Sciences and Applied Mathematics, North Carolina State College; 1961.
[36] Sneddon IN. Relation between load and penetration in axisymmetric Boussinesq problem for punch of arbitrary profile. Int J Eng Sci 1965;3:47–57.
[37] Fischer-Cripps AC. Introduction to contact mechanics. Ann Arbor (MI): Edwards Brothers Inc.; 2000.
[38] Lakes R. The time-dependent Poisson's ratio of viscoelastic materials can increase or decrease. Cell Polym 1992;11:466–9.
[39] Lakes RS, Wineman A. On Poisson's ratio in linearly viscoelastic solids. J Elast 2006;85(1):45–63.
[40] Bazant Z. Theory of creep and shrinkage in concrete structures: a precis of recent developments. Mech Today 1975;2:1–93.
[41] Gopalakrishnan K, Neville A, Ghali A. Creep Poisson's ratio of concrete under multiaxial compression. ACI J 1969.
[42] Hannant D. Creep and creep recovery of concrete subjected to multiaxial compressive stress. ACI J 1969.
[43] Jordaan I, Illston J. The creep of sealed concrete under multiaxial compressive stresses. Mag Concr Res 1969;21(69):195–204.
[44] Jordaan I, Illston J. Time-dependent strains in sealed concrete under multiaxial compressive stress. Mag Concr Res 1971;23. 75-6-9-88.
[45] Bernard O, Ulm F, Germaine J. Volume and deviator creep of calcium-leached cement-based materials. Cem Concr Res 2003;33(8):1127–36.
[46] Grasley Z, Lange D. The viscoelastic response of cement paste to three-dimensional loading. Mech Time-Depend Mater 2007;11(1):27–46.
[47] Grasley ZC, Scherer GW, Lange DA, Valenza JJ. Dynamic pressurization method for measuring permeability and modulus: II. Cementitious materials. Mater Struct 2007;40(7):711–21.
[48] Jones CA. Hollow cylinder dynamic pressurization and radial flow through permeability tests for cementitious materials. College Station, Texas A&M University; 2008.
[49] Kjellsen KO, Monsøy A, Isachsen K, Detwiler RJ. Preparation of flat-polished specimens for SEM-backscattered electron imaging and X-ray microanalysis – importance of epoxy impregnation. Cem Concr Res 2003;33(4):611–6.
[50] Oliver W, Pharr G. Improved technique for determining hardness and elastic modulus using load and displacement sensing indentation experiments. J Mater Res 1992;7(6):1564–83.
[51] Cardona M, Chamberlin RV, Marx W. The history of the stretched exponential function. Ann Phys 2007;16(12):842–5.
[52] Vichit-Vadakan W, Scherer GW. Measuring permeability and stress relaxation of young cement paste by beam bending. Cem Concr Res 2003;33(12):1925–32.
[53] Nemecek J, Kopecky L, Bittnar Z. Size effect in nanoindentation of cement paste. Dundee (Scotland, United kingdom): Thomas Telford Services Ltd.; 2005. p. 47–53.
[54] Oehlert GW. A note on the delta method. Am Stat 1992;46(1):27–9.